Hindawi Publishing Corporation
International Journal of Distributed Sensor Networks
Volume 2014, Article ID 540147, 12 pages
http://dx.doi.org/10.1155/2014/540147

Research Article

An Intelligent Fault Detection Method of a Photovoltaic Module Array Using Wireless Sensor Networks

Kuei-Hsiang Chao, Pi-Yun Chen, Meng-Hui Wang, and Chao-Ting Chen

Department of Electrical Engineering, National Chin-Yi University of Technology, No. 57, Section 2, Zhongshan Road, Taiping District, Taichung 41170, Taiwan

Correspondence should be addressed to Kuei-Hsiang Chao; chaokh@ncut.edu.tw

Received 3 November 2013; Accepted 30 March 2014; Published 15 May 2014

Academic Editor: Wan-Young Chung

This study developed a fault diagnosis meter based on a ZigBee wireless sensor network (WSN) for photovoltaic power generation systems. First, the Solar Pro software was used to simulate the 9-series, 2-parallel photovoltaic module array formed with the Sharp NT-R5E3E photovoltaic module as well as record the power generation data of the photovoltaic module array at different levels of solar radiation, module temperature, and fault conditions. The derived data were used to establish the weights of the extension neural network (ENN). The fault diagnosis in the photovoltaic power generation system required extracting the system's power generation data and real-time solar radiation and module temperatures; this study thus developed an acquisition circuit for measuring these characteristic values. This study implemented extension neural network theory using a PIC single chip microcontroller and incorporated the ZigBee wireless sensor network module to construct a portable fault diagnosis meter to assess the photovoltaic power generation system. The experimental results showed that the proposed portable fault diagnosis meter based on the extension neural network for the photovoltaic power generation system possessed a high level of accuracy in fault identification.

1. Introduction

The photovoltaic power generation system is a minimally polluting renewable energy source. To improve power-generation efficiency, the system must be installed in a spacious and unshaded area. However, the system's output power may decrease with prolonged operation. Furthermore, as the system is outdoors for long time periods, natural disasters could also cause malfunction in the module. A malfunction in any module of the photovoltaic power generation system reduces output power drastically. Therefore, developing fault diagnosis technology for PV power generation systems can not only increase testing and repair efficiency and improve system power generation reliability but also reduce operating costs. As for current fault diagnosis systems of PV power generation systems, relevant PVSAT projects are proceeding in Germany, Netherlands, and Switzerland [1, 2]. These projects establish a self-fault detection system for grid-connected PV power generation systems for the use in detecting system errors and analyzing causes of errors. However, the development of this system involves the use of meteorological satellites to transmit atmospheric data for cross-checking with data measurements from ground-based meteorological stations in order to provide atmospheric parameters for simulation analysis to raise the overall recognition rate. Using this system for fault detection in stand-alone PV power generation systems is prohibited by the high cost, restricting the range of applications for this diagnosis system and reducing its practicality. In addition, experts have also suggested the use of high frequency reaction measurement [3] and time domain reflectometry (TDR) [4] in fault diagnosis of PV power generation systems. These diagnosis methods involve the use of identified and reflected feedback signals to determine the occurrence of faults and the areas in which faults occur. However, this diagnosis technology requires the use of network analyzers and other additional measurement equipment. The technologies applied in both methods require detailed calculations of the internal wire

and cable lengths of PV modules. Consequently, maintenance engineers must possess sufficient PV power generator-related expert knowledge. Furthermore, if this fault diagnosis technology is applied to large-scale PV power generation systems, cable lengths must be calculated accurately or misjudgment of module fault regions will easily occur. Therefore, the application of this diagnosis technology does not facilitate the convenience of system repair. While the author recently proposed an intelligent PV power generation system fault diagnosis method [5] which achieved a fairly good fault type identification rate, the method remains in the simulation stage and is limited to the types of faults it can identify.

A photovoltaic module malfunction is difficult to detect with naked eyes, and, therefore, each module requires manual testing, taking long hours. Additionally, system operations must be terminated while conducting manual testing to ensure the safety of maintenance personnel. Since the photovoltaic module is expensive, the longer the operations are halted, the more extensive the losses become. Furthermore, photovoltaic power generation systems are installed in less accessible regions, thus compounding the difficulty of manual repairs. The development of a fault diagnosis meter in a photovoltaic power generation system, operated via a wireless sensor network transmission, is therefore a key issue for discussion.

To promote the fault diagnosis accuracy rate, an intelligent fault diagnosis method based on extension theory with neural networks was proposed in this paper. The related works of the proposed extension neural network have been applied in [6–10]. The proposed method has the advantages of less learning time, higher accuracy, and less memory consumption. In addition, a PIC microcontroller and a ZigBee wireless sensor network are combined to reduce the hardware circuit size and conduct remote fault diagnosis.

2. Capture of PV Power Generation System Fault Data

In this paper, a 3.15 kW PV power generation system consisting of NT-R5E3E PV modules connected into 9×2 series-parallel is constructed by Solar Pro software package for testing [11]. The Solar Pro software can set the module type, quantity, and installation angle for PV power generation systems. This software is also capable of simulating the *I-V* and *P-V* curves of PV power generation systems in shadow or with faults and even power generation over one day, one month, or one year.

Figure 1(a) shows the *I-V* and *P-V* curves provided in the datasheet for Sharp PV module NT-R5E3E for irradiation from 200 W/m^2 to 1,000 W/m^2 and surface temperature of 25°C [12]; Figure 1(b) shows the *I-V* and *P-V* curves as simulated by Solar Pro PV system analysis software for Sharp solar power module NT-R5E3E under irradiation from 200 W/m^2 to 1,000 W/m^2 and surface temperature of 25°C. Comparison of Figures 1(a) and 1(b) demonstrates that the results simulated by Solar Pro are completely consistent with the figures of the datasheet. It is confirmed that the characteristic curves simulated by Solar Pro are consistent with the actual working characteristic curves and power generation data.

Figure 2 shows the simulated *I-V* and *P-V* curves when two modules in a 3.15 kW PV module array are completely shadowed under irradiation of 900 W/m^2 and surface temperature of 51.6°C. It can be seen from Figure 2 that when a PV module is shadowed, the *I-V* curve is no longer a smooth curve and that multiple peaks are produced in the *P-V* curve. Figure 3 shows the actual measured results under irradiation of 945 W/m^2 and surface module temperature of 51.6°C when two modules in a series array of PV modules are shadowed. It can be seen from Figure 2 that the *I-V* curve changes and multiple peaks are produced in the *P-V* curve. It is evident from Figures 2 and 3 that simulation results are fairly consistent with actual testing results, demonstrating that *I-V* and *P-V* curves experience changes when any module in a PV power generation system is shadowed or faulted; the voltage, current, and power of the maximum power point also change. Consequently, voltage of maximum power point V_{pm}, current of maximum power point I_{pm}, power of maximum power point P_m, and open circuit voltage V_{oc} were selected as the fault diagnosis characteristics by which faults and fault types of PV module array are diagnosed in this paper.

3. Fault Diagnosis Configuration of a Photovoltaic Power Generation System

3.1. Division of Operation Regions. As irradiation and temperature change over time, the module temperature and irradiation ranges that potentially appear through a day are categorized into 21 categories. Between 300 W/m^2 and 1,000 W/m^2, every 100 W/m^2 is designated as one interval. Each interval is then divided into three subintervals every 10°C between 31°C and 60°C. Categories are shown in Table 1.

The fault diagnosis method for PV power generation systems discussed in this paper first requires obtaining the current irradiation and module temperature of the PV module array and then using that information together with the characteristics captured for PV power generation system fault diagnosis, including the maximum output power P_m, voltage of maximum power point V_{pm}, current of maximum power point I_{pm}, and open circuit voltage V_{oc} of the photovoltaic module array during operation. Finally, the proposed extension neural network fault diagnosis method is used to identify whether the PV power generation system is operating normally or a fault has occurred.

3.2. Fault Types of PV Power Generation Systems. Under identical irradiation and module temperature conditions, this paper divides fault categories of PV power generation systems into 10 different types, as shown in Table 2. In addition, the upper and lower limits of the classical domain between irradiation of 301 W/m^2 and 1,000 W/m^2 and module temperature between 31°C and 40°C for 21 regions under 10 different types can be obtained from simulation results.

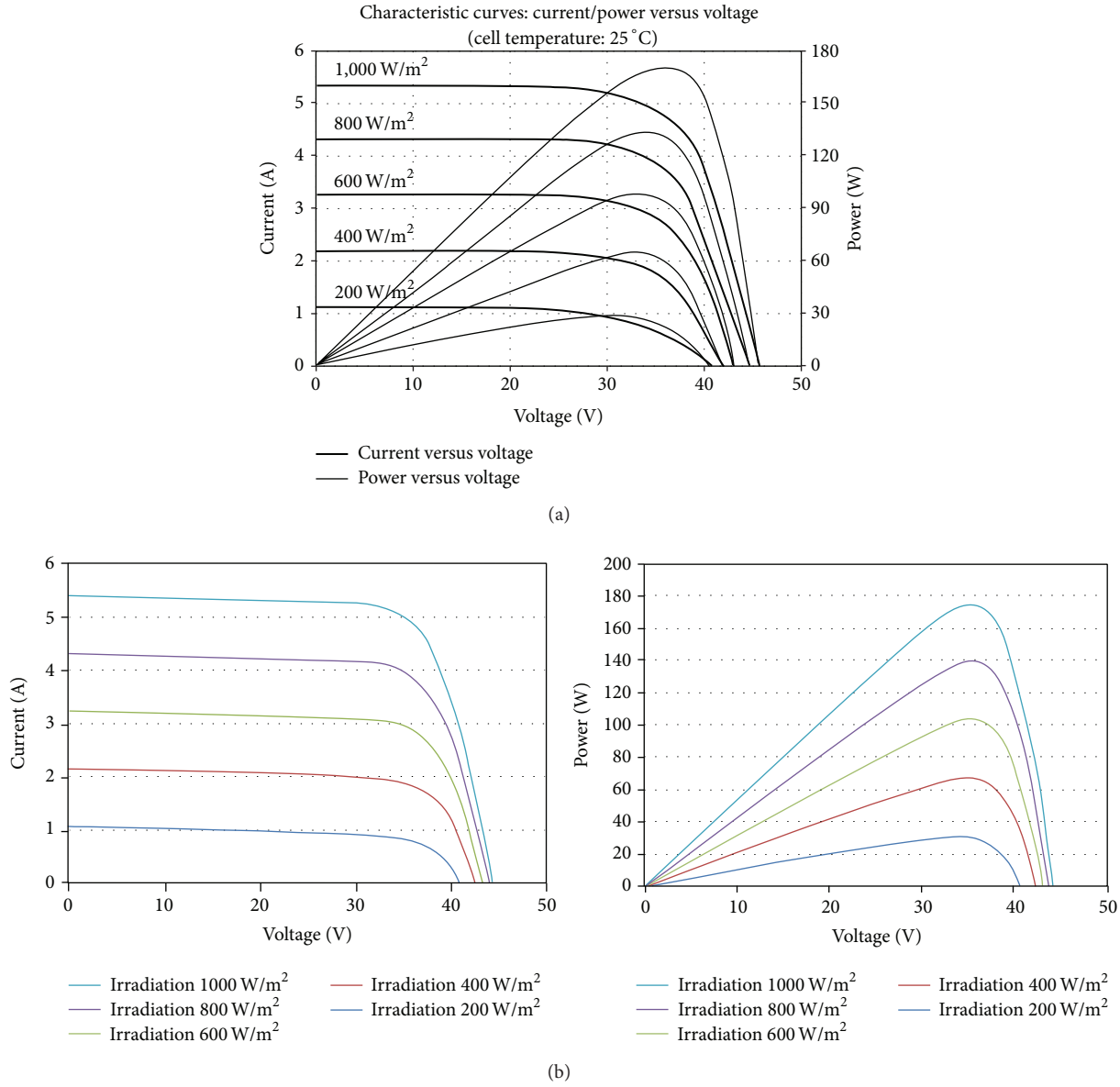

Figure 1: Characteristic curves for surface temperature of 25°C and irradiation from 200 W/m^2 to 1000 W/m^2 (a) provided in Sharp NT-R5E3E datasheet and (b) simulated by Solar Pro software.

3.3. PIC Single Chip Microcontroller. The single chip microcontroller used in this study was the PIC18F8720 microcontroller manufactured by Microchip [13]. This study used a universal asynchronous receiver/transmitter (USART) in the PIC18F8720 single chip microcontroller to transmit data and control operation of a ZigBee module. The ZigBee wireless sensor network module uses a RS-232 communication protocol to transmit data, to contribute to the communication between PIC and ZigBee module. A RS-232 transmission program was coded in the PIC to facilitate communication with the ZigBee module, to control the ZigBee module's operations, and to transmit the photovoltaic power generation system data from the ZigBee wireless sensor network router to the PIC microcontroller for processing.

3.4. ZigBee Wireless Sensor Network. ZigBee is a wireless network protocol based on IEEE 802.15.4 and formulated by the ZigBee Alliance [14, 15]. This wireless sensor network technology is short in distance, simple in structure, low in power consumption, and slow in transmission speed [16–19]. This study used a durable FT-6260 ZigBee Mesh rapid development kit [20] with a transmission distance three to five times greater than the regular ZigBee module. Since each ZigBee module is equipped with a RS-232 transmission port, users can connect the ZigBee module to a computer, facilitating the setting of ZigBee module parameters. Additionally, each ZigBee development module is equipped with four digital input/output (DIO) ports and four analog to digital converters (ADCs). On the DIO side, the ZigBee coordinator

Corp.: Sharp Module: NT-R5E3E String (Series × parallel): 9×2capacity: 3.15 (kW)
Official Parameters: P_{max} = 175.00 (W) V_{pmax} = 35.40 (V) I_{pmax} = 4.95 (A) V_{oc} = 44.40 (V) I_{sc} = 9.84 (A)
Simulation Results: P_{max} = 2085.17 (W) V_{pmax} = 233.70 (V) I_{pmax} = 8.92 (A) V_{oc} = 382.03 (V) I_{sc} = 9.84 (A)
(irradiance 0.90 (kW/m2), Shade Density 100(%))

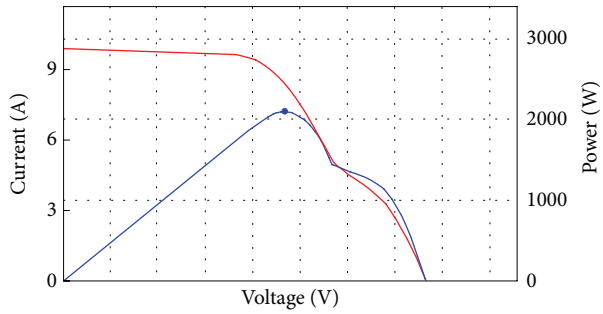

Figure 2: *I-V* and *P-V* curves obtained in simulation under 900 W/m^2 irradiation and surface temperature of 51.6°C where two modules in a PV module array are shadowed.

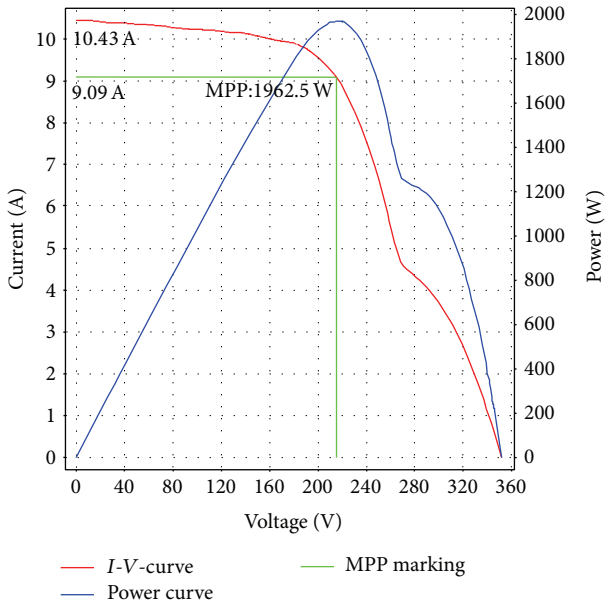

Figure 3: Actual *I-V* and *P-V* curves obtained under 945 W/m^2 irradiation and surface temperature of 51.6°C where two modules in a PV module array are shadowed.

Table 1: 21 regions divided by temperature and irradiation intervals.

Irradiation	Module temperature	Region
301–400 W/m^2	31–40°C	A_1
	41–50°C	A_2
	51–60°C	A_3
401–500 W/m^2	31–40°C	B_1
	41–50°C	B_2
	51–60°C	B_3
501–600 W/m^2	31–40°C	C_1
	41–50°C	C_2
	51–60°C	C_3
601–700 W/m^2	31–40°C	D_1
	41–50°C	D_2
	51–60°C	D_3
701–800W/m^2	31–40°C	E_1
	41–50°C	E_2
	51–60°C	E_3
801–900W/m^2	31–40°C	F_1
	41–50°C	F_2
	51–60°C	F_3
901–1000W/m^2	31–40°C	G_1
	41–50°C	G_2
	51–60°C	G_3

terminal can control the DIO pins at any router end or end-device end on the same network and can also change the voltage level at DIO pins from high voltage to low voltage, or vice versa. On the ADC side, the selected ADC resolution was 12 bits, which allowed for conversion of the 0~2.4 V voltage range into 000~4095(000~FFF) digital data.

3.5. The Sensor Circuit of Characteristic Extraction. The characteristics used to diagnose faults in the photovoltaic power generation system are the maximum output power P_m, voltage of maximum power point V_{pm}, current of maximum power point I_{pm}, and open circuit voltage V_{oc} of the photovoltaic module array. Figure 4 shows the characteristic data extraction circuits. This study uses the ZigBee coordinator module of the fault diagnosis meter in the photovoltaic power generation system to control the remote router DIO at low voltage level, allowing the solid state relay (SSR) to dissociate the photovoltaic module array and the power conditioner, to measure the open circuit voltage of the photovoltaic module array. However, the 400 V maximum open circuit voltage of the photovoltaic module array exceeds the maximum input value of 2.4 V for the ZigBee module. To limit the maximum open circuit voltage of the photovoltaic module array to within the maximum ADC input value of 2.4 V for the ZigBee

Table 2: Fault types of PV power generation systems.

Fault type	Fault condition
PF1	Normal operation
PF2	Of two series branches, a fault has occurred in a module in either of the two branches
PF3	Of two series branches, a fault has occurred in two modules in one branch
PF4	Of two series branches, a fault has occurred in three modules in one branch
PF5	Of two series branches, a fault has occurred in one module in each branch
PF6	Of two series branches, a fault has occurred in two modules in each branch
PF7	Of two series branches, a fault has occurred in three modules in each branch
PF8	Of two series branches, a fault has occurred in one module in one branch and in two modules in the other branch
PF9	Of two series branches, a fault has occurred in one module in one branch and in three modules in the other branch
PF10	Of two series branches, a fault has occurred in two modules in one branch and in three modules in the other branch

module, the photovoltaic module array's output voltage is processed through the series connection of 2 M Ω and 12 K Ω, compressing the maximum open circuit voltage of 400 V into 2.4 V. Following the above method, through ZigBee wireless sensor network transmission, we are able to input the photovoltaic module array's open circuit voltage into the fault diagnosis meter in the photovoltaic power generation system to conduct fault diagnosis. Additionally, 2 M Ω and 12 K Ω resistors prevent loading effects and improve the voltage division accuracy. Using the same method to set the ZigBee wireless sensor network router DIO at high voltage level and then to facilitate SSR conduction and connect the photovoltaic module array and power conditioner in parallel. Owing to the ZigBee module's minimal power output, the SSR cannot be turned on directly, constructing an operation amplifier to boost power and connect the photovoltaic module array to the power conditioner. Then, the power conditioner is equipped with maximum power point tracking (MPPT) and can obtain the voltage of maximum power point, the current of maximum power point, and the maximum power (obtained by multiplying the previous two entities) of the photovoltaic module array by using the voltage sensor and the hall current sensor.

4. Fault Diagnosis in a Photovoltaic Power Generation System

4.1. The Overall Scheme of the Proposed Portable Fault Diagnosis Meter. Figure 5 displays the overall scheme of the proposed portable fault diagnosis meter in the photovoltaic power generation system. The ZigBee module in the fault diagnosis meter controls the conduction of the SSR on the characteristic value acquisition circuit to extract the voltage of maximum power point, current of maximum power point, open circuit voltage, solar radiation, and module temperatures of the photovoltaic module array. The ZigBee wireless Internet transmits the voltage, current, solar radiation, and module temperature values to the fault diagnosis meter, and the diagnosis results and extracted statistics are shown on the LCD.

4.2. The Proposed Extension Neural Network Fault Diagnosis Method. Most of the previously presented results in intelligent neural network design used traditional learning methods for tuning the network parameters [21–25]. However, in this paper, an intelligent method with more efficient learning process was proposed. The characteristics used to diagnose faults in the photovoltaic power generation system are the maximum output power P_{m}, voltage of maximum power point V_{pm}, current of maximum power point I_{pm}, and open circuit voltage V_{oc} of the photovoltaic module array. Because multiple characteristics were used, the proposed method can avoid the inaccuracy in diagnosis caused by the changes in internal electric quantity with temperature and age of a photovoltaic module. The selected characteristics of photovoltaic module arrays are utilized to construct an intelligent diagnosis method according to the extension theory [26] and a modified neural network [27].

The matter-element model and extension distance are the main principles of the proposed extension neural network, which can indicate the alterable relations between quality and quantity by matter-element transformation. The proposed fault detection method will first create a set of fault matter-element model of a photovoltaic module array by extension neural network learning process. And, a regular extension distance will then identify the fault type of a photovoltaic module array by calculating the distance between test data and each matter-element model. According to these results, the proposed fault detection method can detect the fault type of a photovoltaic module array correctly and promptly. The related works of the proposed extension neural network have been successfully applied in [6–10].

Figure 6 presents a structural diagram of the proposed extension neural network. The data are classified and entered into the neural cells of input layers. The number of input layer neural cells is decided by the number of the characteristics of the matter-elements to be identified. Conversely, the output layers are used to store calculated extension distances, and the lines connecting the two layers display the weight, which comprises the upper weight, the center weight, and the lower weight. Finally, the minimum extension distance is identified via the various extension distances stored in the output layers for classification [6–10].

4.3. Learning Process of Extension Neural Network. Before conducting the learning processes, the samples were defined

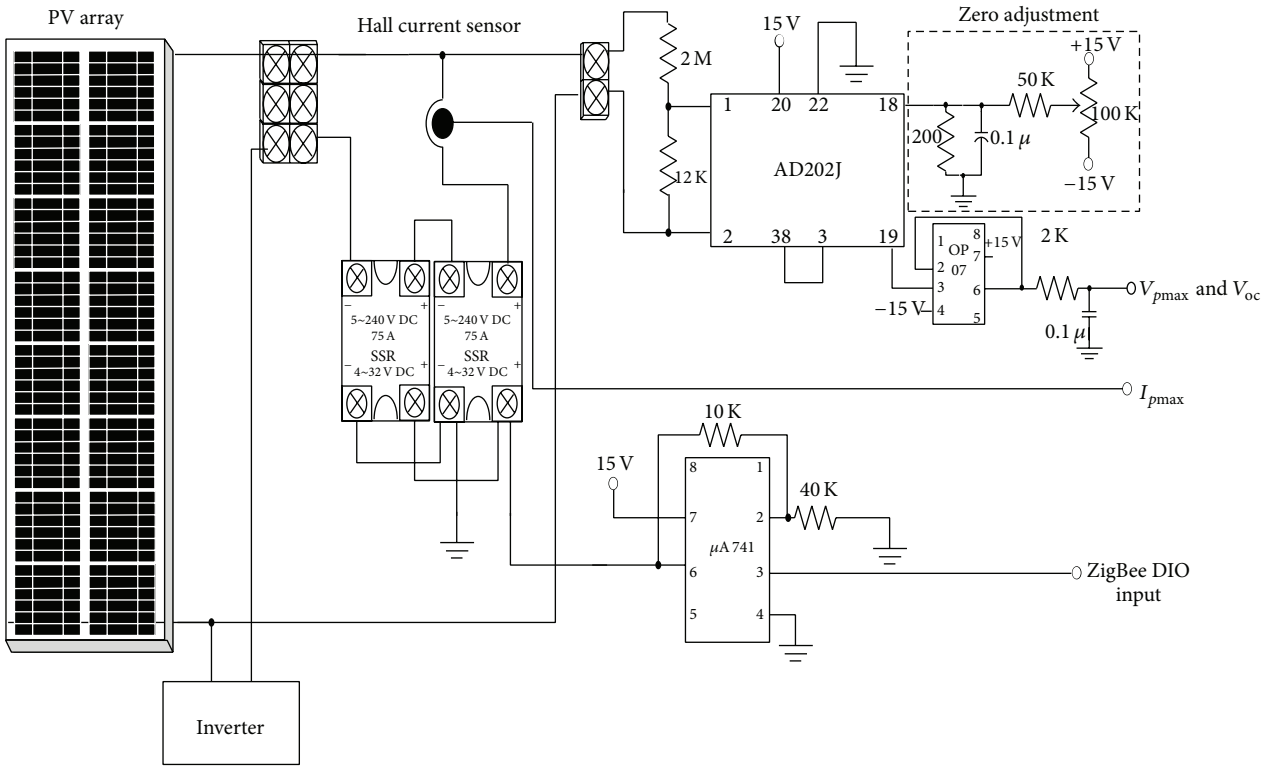

Figure 4: Acquisition circuit of maximum power, maximum power voltage, maximum power current, and open circuit voltage.

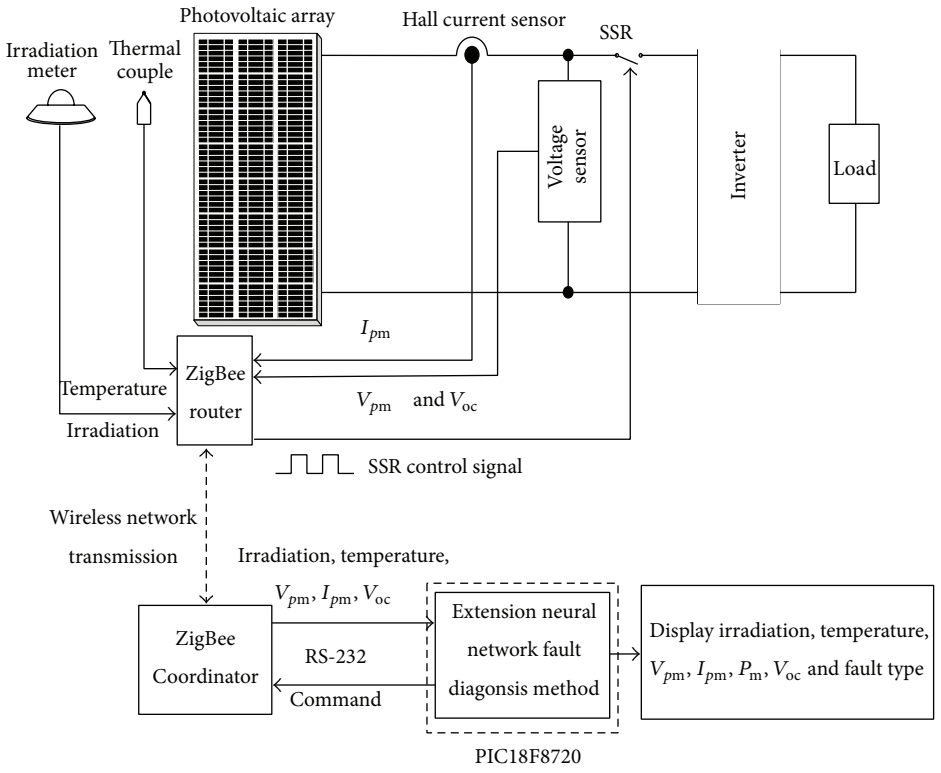

Figure 5: Overall hardware construct of the fault diagnosis meter of portable photovoltaic power generation system.

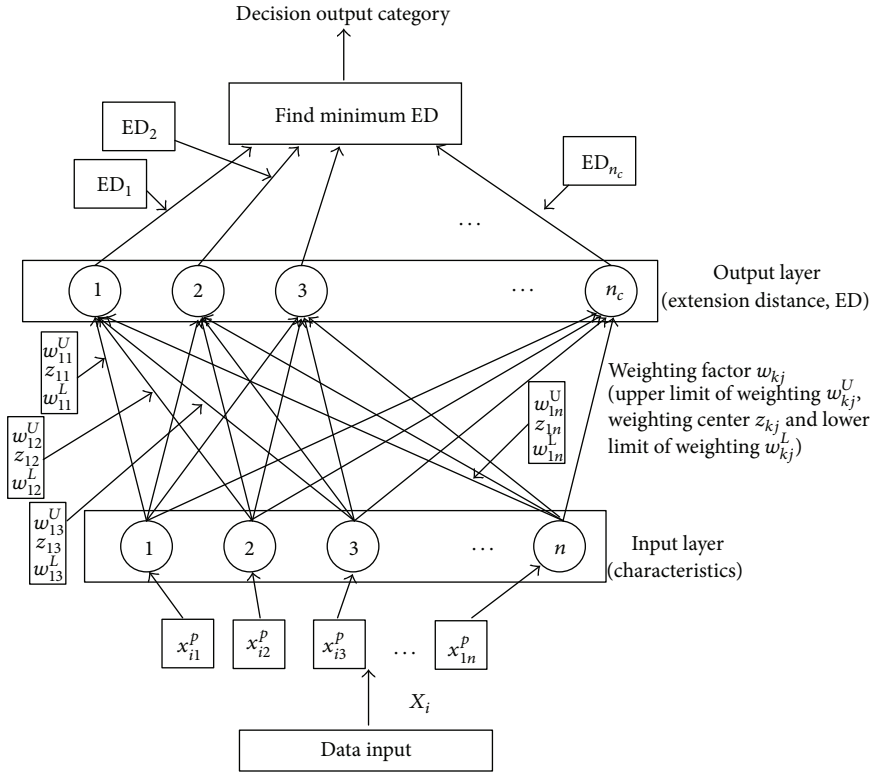

Figure 6: Structure of the proposed extension neural network.

as $X = \{X_1, X_2, X_3, \ldots, X_{T_N}\}$. T_N refers to the total number of samples, each comprised of data characteristics and classifications. Consider $X_i^k = \{X_{i1}^k, X_{i2}^k, X_{i3}^k, \ldots, X_{in}^k\}$, where the learning samples are denoted by $i = 1, 2, 3, \ldots, T_N$, n refers to the total number of characteristics in the matter-element model, k refers to the sample data classification, and the error ratio E_T is defined as

$$E_T = \frac{T_M}{T_N}, \tag{1}$$

where T_M refers to the total error number of classification.

The supervised learning algorithm processes of the extension neural network are detailed as follows.

Step 1. Input the learning data to establish matter-element models that correspond to the different classifications and establish weights between the input and output layers. The kth matter-element is presented as follows:

$$R_k = \begin{bmatrix} N_k, & c_1, & v_{k1} \\ & c_2, & v_{k2} \\ & \vdots & \vdots \\ & c_j, & v_{kj} \end{bmatrix}, \qquad j = 1, 2, 3, \ldots, n;\ k = 1, 2, 3, \ldots, m, \tag{2}$$

where m is the total number of data classifications, c_j is the jth characteristic of the N_kth classification, and v_{kj} is the classical region $\langle w_{kj}^L, w_{kj}^U \rangle$ of the c_j characteristic of the N_kth classification. The range of the classical region can be decided by the learning data and w_{kj}^U and w_{kj}^L are defined as

$$w_{kj}^U = \max_{i \in T_N} \left\{ x_{ij}^k \right\}, \qquad w_{kj}^L = \min_{i \in T_N} \left\{ x_{ij}^k \right\}, \tag{3}$$

where x_{ij}^k refers to the learning data inputted into the extension neural network.

Step 2. Calculate the center weight of each classification characteristic. Consider

$$Z_k = \{z_{k1}, z_{k2}, z_{k3}, \ldots, z_{kn}\}, \qquad z_{kj} = \frac{\left(w_{kj}^U + w_{kj}^L\right)}{2}, \tag{4}$$

where $j = 1, 2, \ldots, n$ and $k = 1, 2, \ldots, m$.

Step 3. Extract the ith learning sample of the kth classification as shown in

$$X_i^k = \left\{ x_{i1}^k, x_{i2}^k, x_{i3}^k, \ldots, x_{in}^k \right\}. \tag{5}$$

Step 4. Use (6) to calculate the extension distance between the learning sample x_{ij}^k and the various classifications. Consider

$$\mathrm{ED}_{ik} = \left[\sum_{j=1}^{n} \frac{\left| x_{ij}^k - z_{kj} \right| - \left(\left(w_{kj}^U - w_{kj}^L \right) / 2 \right)}{\left| \left(w_{kj}^U - w_{kj}^L \right) / 2 \right|} + 1 \right], \tag{6}$$

$$k = 1, 2, \ldots, m,$$

where x_{ij}^{k} refers to the jth characteristic of the ith learning sample of the kth classification, z_{kj} refers to the center weight between the jth input and the kth output, and w_{kj}^{U} and w_{kj}^{L} refer to the upper and lower weight limits between the jth input and the kth output.

Step 5. Find the minimum extension distance between all the classifications in the output layer. If $\mathrm{ED}_{ik}^{*} = \min_{k\in m}\{\mathrm{ED}_{ik}\}$, then classification k^{*} and data classification k are the same ($k^{*} = k$), denoting the identification was correctly conducted, and Step 7 should be conducted directly. If the extension distance $\mathrm{ED}_{ik}^{*} \neq \min_{k\in m}\{\mathrm{ED}_{ik}\}$, denoting the classification k^{*} differs from data classification k ($k^{*} \neq k$), the learning processes in Step 6 should be fulfilled.

Step 6 (adjust the weights). (1) Modify the upper and lower weights.

Modify the weight of the classification k to obtain

$$\begin{aligned} w_{kj\_\mathrm{new}}^{L} &= w_{kj\_\mathrm{old}}^{L} + \eta\left(x_{ij}^{k} - z_{kj\_\mathrm{old}}\right), \\ w_{kj\_\mathrm{new}}^{U} &= w_{kj\_\mathrm{old}}^{U} + \eta\left(x_{ij}^{k} - z_{kj\_\mathrm{old}}\right). \end{aligned} \tag{7}$$

Modify the weight of the classification k^{*} to obtain

$$\begin{aligned} w_{k^{*}j\_\mathrm{new}}^{L} &= w_{k^{*}j\_\mathrm{old}}^{L} - \eta\left(x_{ij}^{k} - z_{k^{*}j_{\mathrm{old}}}\right), \\ w_{k^{*}j\_\mathrm{new}}^{U} &= w_{k^{*}j\_\mathrm{old}}^{U} - \eta\left(x_{ij}^{k} - z_{k^{*}j_{\mathrm{old}}}\right). \end{aligned} \tag{8}$$

(2) Modify the center weight

$$\begin{aligned} z_{kj\_\mathrm{new}} &= \frac{\left(w_{kj\_\mathrm{new}}^{U} + w_{kj\_\mathrm{new}}^{L}\right)}{2}, \\ z_{k^{*}j\_\mathrm{new}} &= \frac{\left(w_{k^{*}j\_\mathrm{new}}^{U} + w_{k^{*}j\_\mathrm{new}}^{L}\right)}{2}, \end{aligned} \tag{9}$$

where η is the learning rate of the extension neural network, $w_{kj\_\mathrm{new}}^{U}, w_{kj\_\mathrm{new}}^{L}$ are the upper and lower weights of the jth characteristic in the kth classification after learning, $w_{k^{*}j\_\mathrm{new}}^{U}, w_{k^{*}j\_\mathrm{new}}^{L}$ are the upper and lower weights of the jth characteristic in the k^{*}th classification after learning, $w_{kj\_\mathrm{old}}^{U}, w_{kj\_\mathrm{old}}^{L}$ are the upper and lower weights of the jth characteristic in the kth classification before learning, $w_{k^{*}j\_\mathrm{old}}^{U}, w_{k^{*}j\_\mathrm{old}}^{L}$ are the upper and lower weights of the jth characteristic in the k^{*}th classification before learning, $z_{kj\_\mathrm{old}}, z_{k^{*}j\_\mathrm{old}}$ are the center weight of the jth characteristic in the kth and k^{*}th classification before learning, and $z_{kj\_\mathrm{new}}, z_{k^{*}j\_\mathrm{new}}$ are the center weight of the jth characteristic in the kth and k^{*}th classification after learning.

Step 7. The learning processes are terminated upon completed classification of all the learning samples. Otherwise, repeat Steps 3 to 6.

Step 8. When the total error ratio E_T reaches the expected value, the learning classification procedures are terminated. Otherwise, repeat Step 3 to resume the learning and training procedures.

Figure 7 shows the adjustment process of the weighting factors, as described in Step 6. The learning sample x_{ij}, in Figure 7(a), belongs to cluster B. However, the result of the extension distance equation is $\mathrm{ED}_A < \mathrm{ED}_B$; thus, it is classified as cluster A. As shown in Figure 7(b), after the adjustment of the weighting factor, the new extension distance is $\mathrm{ED}'_A > \mathrm{ED}'_B$; hence, the learning sample x_{ij} can be classified as cluster B.

4.4. The Recognition Algorithm Processes of the ENN. Upon completion of the extension neural network, the learning processes, recognition, diagnosis, and classification can be implemented. The procedures are as follows [6–10].

Step 1. Extract the weight matrix of the trained extension neural network.

Step 2. Extract the samples awaiting recognition.

Step 3. Use (6) to calculate the extension distance between the samples awaiting identification and each classification.

Step 4. Find the minimum extension distance to identify the classification of each data awaiting identification.

Step 5. Check that all samples awaiting identification are tested before the algorithm is terminated. Otherwise, repeat Step 2 to process the next sample awaiting identification.

The characteristics used to diagnose faults in the photovoltaic power generation system are the maximum output power P_{m}, voltage of maximum power point V_{m}, current of maximum power point $I_{p\mathrm{m}}$, and open circuit voltage V_{oc} of the photovoltaic module array. Therefore, there are four parameters fed to the neural network. Under identical irradiation and module temperature conditions, this paper divides fault categories of PV power generation systems into 10 different types, as shown in Table 2. There are 2,196 entries of data collected from the photovoltaic module array for 10 different types that were divided into 1,098 entries of training data and 1,098 test data. The 1,098 entries of training data were used for the extension neural network training process introduced in Section 4.3. Therefore, the vector lengths of data from the cells unit are 1,098. In this study, (6) is used to calculate the extension distance ED_{ik} between the learning sample x_{ij}^{k} and the various classifications. After that, the minimum extension distance between all the classifications in the output layer is found. If $\mathrm{ED}_{ik}^{*} = \min_{k\in m}\{\mathrm{ED}_{ik}\}$, then classification k^{*} and data classification k are the same ($k^{*} = k$), denoting the identification was correctly conducted, and the learning processes are terminated upon completed classification of all the learning samples. However, if the extension distance $\mathrm{ED}_{ik}^{*} \neq \min_{k\in m}\{\mathrm{ED}_{ik}\}$, denoting the classification k^{*} differs from data classification k ($k^{*} \neq k$), the weights adjusting process should be fulfilled. Therefore, the extension distances ED_{ik} between the learning sample x_{ij}^{k} and the various classifications are the feedback controlled elements.

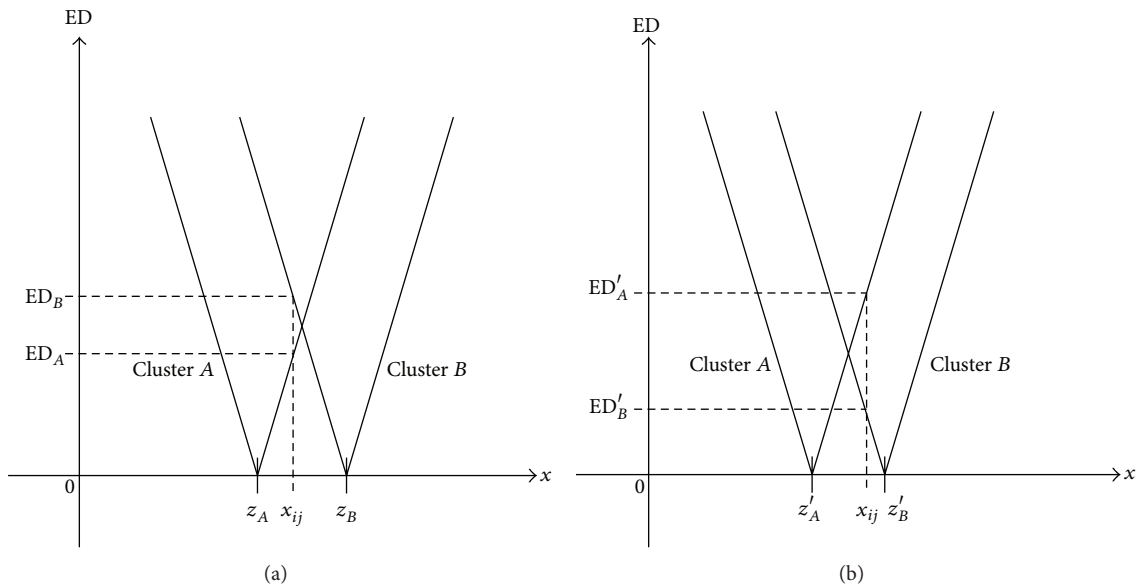

FIGURE 7: Adjustment process of cluster weighting: (a) before learning and (b) after learning.

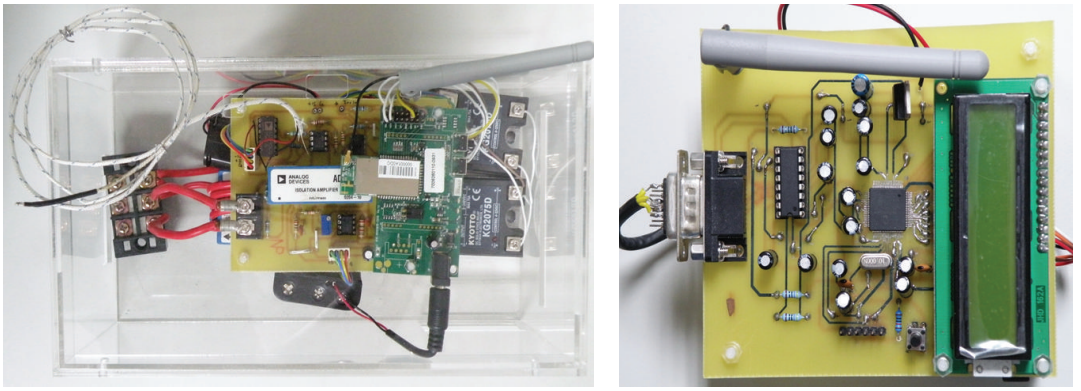

FIGURE 8: Hardware photos of the PV fault diagnosis meter: (a) the characteristic value acquisition circuit and ZigBee wireless internet module combination and (b) the combined ZigBee coordinator and PIC microcontroller circuits.

5. Experimental Results

Figure 8(a) demonstrates the hardware photo of the combined characteristic value acquisition circuit and ZigBee wireless internet module. In addition to requiring a fault diagnosis program on the PIC single chip microcontroller of the photovoltaic power generation system, a transmitted control signal is also essential for controlling the ZigBee module. ZigBee uses the 12 V input and output voltage RS-232 communication protocol. Without an input and output voltage lower than 12 V, the PIC single chip microcontroller requires a Max232IC on the fault diagnosis meter to communicate with the ZigBee module and control its operations. The generator data transmitted by the ZigBee module to the photovoltaic power generation system is inputted into the PIC microcontroller chip for concurrent processing. Figure 8(b) shows the hardware photo of the combined ZigBee coordinator and PIC microcontroller circuits in the photovoltaic power generation system.

To determine the proposed extension neural network's feasibility for photovoltaic power generation system fault diagnosis, this study employed test data with a solar radiation between 901 W/m^2 and 1,000 W/m^2 and module temperatures between 31°C and 40°C. Table 3 displays the simulated data from Solar Pro [11] and their transmitted data from the ZigBee module ADC, making the transmitted statistics the data for actual test. The table demonstrates that the proposed extension neural network accurately diagnosed the photovoltaic power generation system faults. Despite discrepancies between the data generated via the Solar Pro software and the transmitted data from the ZigBee module ADC, Table 3 indicates only one datum (item number 3) was incorrectly assessed, thereby proving a high-identification rate.

Table 3: Test data with a solar radiation between 901 W/m^2 and 1,000 W/m^2 and module temperatures between 31°C and 40°C, data transmitted to ZigBee, known fault types, and the results of extension neural network fault diagnosis.

Item number	Simulated data of Solar Pro				Data transmitted of ZigBee				Known fault type	Diagnosed fault type
	P_m	V_{pm}	I_{pm}	V_{oc}	P_m	V_{pm}	I_{pm}	V_{oc}		
1	3116.6	314.66	9.9	396.08	3134	316	9.8	397	PF1	PF1
2	2872.7	291.21	9.86	396.02	2890	293	9.8	397	PF2	PF2
3	2539.8	255.57	9.94	396.03	2559	257	9.9	397	**PF3**	**PF2**
4	1944.71	218.99	8.8	390.39	1961	220	8.8	392	PF4	PF4
5	2463.83	278.09	8.86	347.05	2480	279	8.8	348	PF5	PF5
6	2156.42	242.16	8.9	330.68	2172	244	8.8	305	PF6	PF6
7	1847.94	206.17	8.96	260.29	1864	208	8.9	262	PF7	PF7
8	2241.85	250.56	8.95	347.01	2260	252	8.9	348	PF8	PF8
9	1940.26	218.82	8.87	347.01	1958	220	8.8	348	PF9	PF9
10	1925.53	218.11	8.83	303.63	1942	220	8.8	305	PF10	PF10

Upon conducting a local feasibility analysis of the extension neural network for fault diagnosis in a photovoltaic power generation system, the method's accuracy under different solar radiation and module temperature conditions must be measured. Table 4 shows the fault diagnosis results of randomly chosen test data and indicates that the diagnosis accuracy remained high under various solar radiation and module temperature conditions. The proposed use of the extension neural network for fault diagnosis in a photovoltaic power generation system involves minimal training and simple learning processes and is, therefore, suitable for fault diagnosis in a photovoltaic power generation system.

The fault classification characteristic values of test data with a solar radiation value between 901 W/m^2 and 1,000 W/m^2 and module temperatures between 31°C and 40°C and those with a solar radiation value between 601 W/m^2 and 700 W/m^2 and module temperatures between 31°C and 40°C are too similar. This resulted in diagnosis errors and reduced accuracy rates to only 96% and 92%, lower than those in other regions. However, only these two regions observed lower accuracy rates; the rates in other regions were 100%.

To display the superiority of the proposed extension neural network, fuzzy neural network [25] and multilayer perceptrons and back propagations (MLP) [21] with three network structures, namely, 4-7-10, 4-8-10, and 4-9-10 (input layer-hidden layer-output layer), were constructed to diagnose photovoltaic module array faults and to compare diagnosis results of the extension neural network, as seen in Table 5. The fault diagnosis of photovoltaic module arrays divided solar radiation and module temperatures into 21 regions, conducting a diagnostic simulation of each region. The fault diagnosis displayed in Table 5 demonstrates a higher identification performance by the proposed extension neural network compared with that of multilayer perceptrons and back propagation diagnosis and only requires 22 iterations, indicating that each region only requires approximately 1 iteration to reach a 100% identification rate. Conversely, fuzzy neural network and multilayer perceptrons and back propagations require at least 5,584 and 8,507 iterations, respectively, indicating that each region requires an average of 250 and 400 iterations to reach a neural network convergence. The comparison results indicate that an extension neural network conducting fault diagnosis is highly accurate and requires minimal iterations and is, therefore, more efficient than traditional multilayer perceptrons and back propagation diagnosis.

Table 5 shows that the proposed method suits better the practical situation due to the effects of photovoltaic module aging being considered. The proposed extension neural network only needs the basic computing rules such as addition, subtraction, multiplication, and division. Compared with the neural network method presented in [21] and fuzzy neural network proposed in [25], the learning and diagnosis response of the proposed extension neural network is also faster under the same conditions. It is because more complex computing instruction such as exponential function is needed using the traditional neural network and fuzzy neural network methods. However, the proposed extension neural network diagnosis method does not need complex learning procedure, such that it can easily be implemented on a single chip microcontroller. However, when the capacity of photovoltaic modules increases or reduces, a fractional amount of the classical region data should be modified to promote the diagnosis accuracy. Because the diagnosis scheme is simple, a PIC microcontroller can be utilized to implement the hardware for real-time fault diagnosis of a photovoltaic module array. There are a lot of analog and digital modules in the PIC microcontroller, so it makes the hardware circuit size very small.

The characteristics used to diagnose faults in the photovoltaic power generation system are the maximum output power P_m, voltage of maximum power point V_{pm}, current of maximum power point I_{pm}, and open circuit voltage V_{oc} of the photovoltaic module array. Because multiple characteristics were used, the proposed method can avoid the inaccuracy in diagnosis caused by the changes in internal electric quantity with temperature and age of a photovoltaic module. However, the proposed fault diagnosis system cannot handle sparks caused by lighting. Fortunately, the lighting sparks can be absorbed by lighting arrester installed on photovoltaic power generation system.

Table 4: Fault diagnosis accuracy rates of the extension neural network in photovoltaic power generation system in different regions.

Irradiation	Module surface temperature	Diagnosis accuracy 1−(error number/total number)
901~1000 W/m^2	31°C~40°C	**1 − 2/50 (=96%)**
	41°C~50°C	1 − 0/50 (=100%)
	51°C~60°C	1 − 0/58 (=100%)
801~900 W/m^2	31°C~40°C	1 − 0/50 (=100%)
	41°C~50°C	1 − 0/50 (=100%)
	51°C~60°C	1 − 0/50 (=100%)
701~800 W/m^2	31°C~40°C	1 − 0/50 (=100%)
	41°C~50°C	1 − 0/50 (=100%)
	51°C~60°C	1 − 0/50 (=100%)
601~700 W/m^2	31°C~40°C	**1 − 4/50 (=92%)**
	41°C~50°C	1 − 0/50 (=100%)
	51°C~60°C	1 − 0/50 (=100%)
501~600 W/m^2	31°C~40°C	1 − 0/55 (=100%)
	41°C~50°C	1 − 0/50 (=100%)
	51°C~60°C	1 − 0/52 (=100%)
401~500 W/m^2	31°C~40°C	1 − 0/55 (=100%)
	41°C~50°C	1 − 0/55 (=100%)
	51°C~60°C	1 − 0/55 (=100%)
301~400 W/m^2	31°C~40°C	1 − 0/55 (=100%)
	41°C~50°C	1 − 0/56 (=100%)
	51°C~60°C	1 − 0/57 (=100%)

Table 5: Comparison of fault diagnosis accuracy rates between test data with a solar radiation between 301 W/m^2 and 1,000 W/m^2 and module temperatures between 31°C and 40°C, when applied in extension neural networks and traditional neural networks.

Method	Comparison item		
	Iteration number	Learning accuracy rate	Diagnosis accuracy rate
Proposed extension neural network (ENN)	22	100%	100%
MLP (4-7-10) [21]	8,507	90.85%	93.33%
MLP (4-8-10) [21]	11,089	85.65%	90%
MLP (4-9-10) [21]	8,597	96.64%	93.33%
Fuzzy neural network [25]	5,584	98.84%	97.70%

6. Conclusions

This study conducted fault diagnosis on photovoltaic power generation systems. First, Solar Pro software was used to develop a 3.15 kW photovoltaic power generation system simulating regular operation and operation under various fault classifications. The characteristic values of the photovoltaic power generation system under both conditions were recorded. Half the simulation results were used as training data to test the weight of the extension neural network, and the PIC single chip microcontroller was used to develop the photovoltaic power generation system's fault diagnosis meter based on an extension neural network. The results indicate a high extension neural network recognition rate, and that minimal learning data is required to complete weight training. Additionally, the combination of a PIC single chip microcontroller and a ZigBee wireless sensor network transmitter greatly reduced the risks involved in manual repairs and reduced the time required for system diagnosis. Furthermore, a ZigBee wireless sensor network transmission can conduct a remote fault diagnosis. Finally, the proposed fault diagnosis meter for photovoltaic power generation systems and the fault characteristic value acquisition circuit are both small in size and light in weight and are therefore portable.

Conflict of Interests

The authors of the paper declare that there is no conflict of interests with any of the commercial identities mentioned in the paper.

Acknowledgment

This work was supported by National Science Council, Taiwan, under Grants NSC 102-2221-E-167-009 and NSC 101-ET-E-167-001-ET.

References

[1] J. Betcke, V. V. Dijk, C. Reise et al., "PVSAT: remote performance check for grid connected PV systems using satellite data, evaluation of one year field-testing," in *Proceedings of the 17th European Photovoltaic Solar Energy Conference*, 2001.

[2] E. Lorenz, J. Betcke, A. Drews et al., "PVSAT-2: intelligent performance check of PV system operation based on satellite data," in *Proceedings of the 19th European Photovoltaic Solar Energy Conference*, 2004.

[3] L. Schirone, F. P. Califano, U. Moschella, and U. Rocca, "Fault finding in a 1 MW photovoltaic plant by reflectometry," in *Proceedings of the 1st IEEE Photovoltaic Specialists Conference*, pp. 846–849, December 1994.

[4] T. Takashima, K. Otani, K. Sakuta et al., "Electrical detection and specification of failed modules in PV array," in *Proceddings of the 3rd World Conference on Photovoltaic Energy Conversion*, pp. 2276–2279, jpn, May 2003.

[5] K. H. Chao, S. H. Ho, and M. H. Wang, "Modeling and fault diagnosis of a photovoltaic system," *Electric Power Systems Research*, vol. 78, no. 1, pp. 97–105, 2008.

[6] M. H. Wang, "Extension neural network for power transformer incipient fault diagnosis," *IET Generation, Transmission & Distribution*, vol. 150, pp. 679–685, 2003.

[7] M. H. Wang and C. P. Hung, "Extension neural network," in *Proceedings of the International Joint Conference on Neural Networks*, pp. 399–403, July 2003.

[8] K. H. Chao, C. L. Chiu, C. J. Li, and Y. C. Chang, "A novel neural network with simple learning algorithm for islanding phenomenon detection of photovoltaic systems," *Expert Systems with Applications*, vol. 38, no. 10, pp. 12107–12115, 2011.

[9] K. H. Chao and J. W. Chen, "State-of-health estimator based-on extension theory with a learning mechanism for lead-acid batteries," *Expert Systems with Applications*, vol. 38, no. 12, pp. 15183–15193, 2011.

[10] K. H. Chao and J. W. Chen, "Design and implementation of a capacity estimator using simple neural networks for lead-acid batteries," *International Review of Electrical Engineering*, vol. 6, no. 7, pp. 2965–2973, 2011.

[11] Solar Pro Brochure and Laplace System Co., 2007, http://www.lapsys.co.jp/english/e_products/e_pamphlet/sp_e.pdf.

[12] Sharp Corporation of Australia, "Sharp NT-R5E3E PV module user menu," 2009, http://www.sharp.net.au/catalogue/brochures/NTR5E3E_1127_brochure.pdf.

[13] "PIC18Fxx20 Data sheet," Microchip Technology Inc., 2003, http://ww1.microchip.com/downloads/cn/DeviceDoc/cn0118-97.pdf.

[14] J. T. Adams, "An introduction to IEEE STD 802.15.4," in *Proceedings of the IEEE Aerospace Conference*, March 2006.

[15] ZigBee Alliance, "ZigBee specification version 1.0," 2004, http://www.zigbee.org.

[16] X. Q. Zhu and J. M. Wang, "The research and implementation of ZigBee protocol network," *Electron Technologies*, vol. 1, pp. 129–132, 2006.

[17] D. Geer, "Users make a beeline for ZigBee sensor technology," *Computer*, vol. 38, no. 12, pp. 16–19, 2005.

[18] L. Y. Yuan and Y. L. Zhu, "Traffic monitoring network simulation of wireless sensor based on NS2," *Journal of System Simulation*, vol. 19, no. 3, pp. 660–664, 2007.

[19] W. Andrew, "Commercial applications of wireless sensor networks using ZigBee," *IEEE Communications Magazine*, vol. 45, no. 4, pp. 70–77, 2007.

[20] "FT-6260 High power ZigBee mesh rapid development kit," in *User Manual*, Surewin Technology Ltd., 2009.

[21] Y. Wu, Q. Lan, and Y. Sun, "Application of BP neural network fault diagnosis in solar photovoltaic system," in *Proceedings of the International Conference on Mechatronics and Automation (ICMA '09)*, pp. 2581–2585, 2009.

[22] C. H. Wang, W. Y. Wang, T. T. Lee, and P. S. Tseng, "Fuzzy B-spline membership function (BMF) and its applications in fuzzy-neural control," *IEEE Transactions on Systems, Man and Cybernetics*, vol. 25, no. 5, pp. 841–851, 1995.

[23] J. S. R. Jang, "Input selection for ANFIS learning," in *Proceedings of the 5th IEEE International Conference on Fuzzy System*, 1996.

[24] C. T. Lin and C. S. G. Lee, *Neural Fuzzy Systems: A Neuro-Fuzzy Synergism to Intelligent Systems*, Prentice-Hall, Englewood Cliffs, NJ, USA, 1999.

[25] S. K. Oh, W. Pedrycz, and H. S. Park, "A new approach to the development of genetically optimized multilayer fuzzy polynomial neural networks," *IEEE Transactions on Industrial Electronics*, vol. 53, no. 4, pp. 1309–1321, 2006.

[26] W. Cai, "The extension set and incompatibility problem," *Journal of Scientific Exploration*, vol. 1, pp. 81–93, 1983.

[27] K. H. Chao, C. J. Li, and M. H. Wang, *A maximum power point tracking method based on extension neural network for PV system*, vol. 5551 of *Lecture Notes in Computer Science*, Springer, 2009.